NANO LETTERS

Letter

pubs.acs.org/NanoLett

Fast Energy Relaxation of Hot Carriers Near the Dirac Point of Graphene

R. Somphonsane,[†] H. Ramamoorthy,[‡] G. Bohra,[‡] G. He,[‡] D. K. Ferry,[§,∥] Y. Ochiai,[∥] N. Aoki,[∥] and J. P. Bird*[,‡,∥]

[†]Department of Physics, University at Buffalo, Buffalo, New York 14260-1500, United States

[‡]Department of Electrical Engineering, University at Buffalo, Buffalo, New York 14260-1900, United States

[§]School of Electrical, Computer, and Energy Engineering, and Center for Solid State Electronics Research, Arizona State University, Tempe, Arizona 85287-5706, United States

[∥]Graduate School of Advanced Integration Science, Chiba University, 1-33 Yayoi-cho, Inage-ku, Chiba 263-8522, Japan

Supporting Information

ABSTRACT: We investigate energy relaxation of hot carriers in monolayer and bilayer graphene devices, demonstrating that the relaxation rate increases significantly as the Dirac point is approached from either the conduction or valence band. This counterintuitive behavior appears consistent with ideas of charge puddling under disorder, suggesting that it becomes very difficult to excite carriers out of these localized regions. These results therefore demonstrate how the peculiar properties of graphene extend also to the behavior of its nonequilibrium carriers.

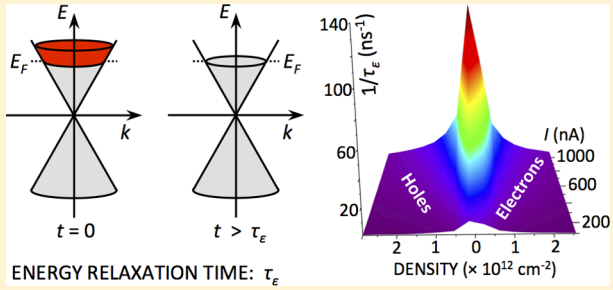

KEYWORDS: *Graphene, hot carriers, energy relaxation, electron−phonon scattering*

The loss of excess energy by "hot" carriers, driven out of equilibrium by optical or electrical excitation, is critical to the operation of modern semiconductor devices.[1,2] With the emergence of graphene as a promising new material for nanoelectronics,[3−6] the need to understand the origins of its energy relaxation has stimulated significant theoretical[7−14] and experimental[15−29] activity. A key aspect of graphene is the large energy of its various optical modes, which ensures that these phonons are ineffective in cooling at all but the highest temperatures. While substrate phonons may provide a path for relaxation,[6] the cooling of hot carriers is primarily achieved through their interaction with acoustic phonons (especially at the low temperatures of interest here). An important parameter for describing this cooling is the energy-relaxation time (τ_ϵ), the typical time on which energy is lost by the carriers as a whole.[1,2] The variation of this parameter with temperature and density can yield valuable insight into the mechanisms responsible for cooling, an issue that is of particular relevance to graphene for which distinct, disorder-dependent, relaxation pathways have been predicted.[7−10,12,13] In this Letter, we therefore determine the energy-relaxation time in this material, utilizing the carrier-heating approach that has previously been applied to conventional semiconductors.[30−32]

Many of the novel properties of graphene derive from the peculiarities of its bandstructure, whose linear energy bands intersect at so-called Dirac points (DPs) where the density of states also vanishes. In contrast to metals with their large Fermi surfaces, a feature of acoustic-phonon scattering in graphene is that the boundary between its "high-" and "low-" temperature regimes is actually dependent upon carrier density, through the influence of this parameter on the Bloch-Gruneisen temperature (T_{BG})[33,34] (we return to this point below). As the Fermi level is swept toward the DP from either band, the phase space available for scattering shrinks and one might therefore expect hot-carrier cooling to slow significantly. However, recent theories for both clean[8] and disordered[13] graphene predict exactly the opposite behavior, arguing that the relaxation rate should increase as the DP is approached. Particular attention has focused on ref 13 in which this surprising behavior was obtained by considering how disorder-mediated scattering may relax momentum-conservation constraints, allowing the full thermal-phonon distribution to be utilized in cooling. These "super-collisions" were found to become particularly effective as the DP is approached, where the Bloch-Gruneisen temperature becomes vanishingly small and one effectively enters the regime of high-temperature phonon scattering. Recent experiments performed using pn-junction photocurrents[27] and noise thermometry[28] appear to provide support for this mechanism.

As has long been known from the study of conventional semiconductors (see refs 30−32, for example), a useful mechanism for investigating hot-carrier cooling involves using a large measurement current to raise the effective carrier

Received: June 7, 2013
Revised: August 13, 2013
Published: August 21, 2013

   dx.doi.org/10.1021/nl4020777 | *Nano Lett.* 2013, 13, 4305−4310

temperature (T_e) above that of the lattice (T_L). In this Letter, we make use of this approach to investigate energy relaxation in graphene, working primarily in the high-density limit ($T_{BG} > T_L$) appropriate for many electronic-device applications. By determining the energy-relaxation time from the dependence of T_e on input power, we demonstrate a pronounced increase in the cooling rate (i.e., $\tau_e \rightarrow 0$) as the DP is approached from either the electron or hole bands. While this behavior is suggestive of recent theories for energy relaxation in graphene,[8,13] our observations imply a stronger quantitative variation than that predicted by these models. At the same time, neither the variation of the power-loss rate nor of the relaxation time with temperature is found to be consistent with their predictions. Our results therefore suggest that the understanding of carrier cooling in this material is still incomplete, and we point to the known strong incompressibility of the electron−hole system at the DP as a possible reason for this. The incompressibility implies that excitation of carriers out of electron and hole puddles should be suppressed as the DP is approached, requiring rapid energy relaxation that will have important consequences for the design of future devices that operate far from equilibrium in this material.

Our graphene devices were fabricated by exfoliating Kish graphite onto a doped Si substrate with a 300 nm SiO_2 cap layer. Further details are provided in ref 35 (where we investigated mesoscopic conductance fluctuations (CF) in monolayer and bilayer flakes) and in the Supporting Information where we demonstrate the basic characterization of our devices. Here, we explore nonlinear transport in three new devices, one of which (M1) was realized from a monolayer flake, while the other two (B1 and B2) were formed in bilayer graphene. (Assignments made on the basis of optical microscopy and Raman spectroscopy.) The devices were contacted with Cr/Au electrodes as indicated in Figure 1a (B1 and B2 had a similar geometry). Key transport parameters for the three devices are summarized in Table 1. Carrier density (n) was varied by means of the voltage (V_g) applied to the conductive Si substrate, and in device M1 Hall measurements were used to reliably determine its value down to a level of $\sim 4 \times 10^{11}$ cm^{-2} (see Supporting Information). A simple parallel-plate capacitor expression was found to yield values within 10% of those obtained from the Hall studies, giving us confidence in applying this formula to devices B1 and B2. In the figures that follow, error bars in the density primarily reflect the difference between these two approaches. All conductance measurements were made by low-frequency (13 Hz) lock-in detection, using a steady ac current whose RMS value was varied from 100 nA to 20 μA.

Previously, we showed that the linear conductance of our graphene devices exhibits mesoscopic fluctuations at low temperatures, whose amplitude is suppressed with increasing T_L[35,36] (also see the Supporting Information, Figures S1−S3). This is also illustrated in Figure 1b in which we show fluctuations at a number of different lattice temperatures (with fixed current of 100 nA). In contrast to this, in Figure 1c we show corresponding features as a function of current (at T_L = 1.8 K). For the purpose of CF thermometry, we determine the RMS fluctuation (δg_{rms}, in units of e^2/h) for each data set by averaging over a small range of V_g that nonetheless contains several fluctuations. By plotting $\delta g_{rms}(T_L)$ and $\delta g_{rms}(I)$ on a common graph, we assign an effective T_e to each value of the current[26] (see Supporting Information). From the average resistance over the same range of V_g, we then determine the

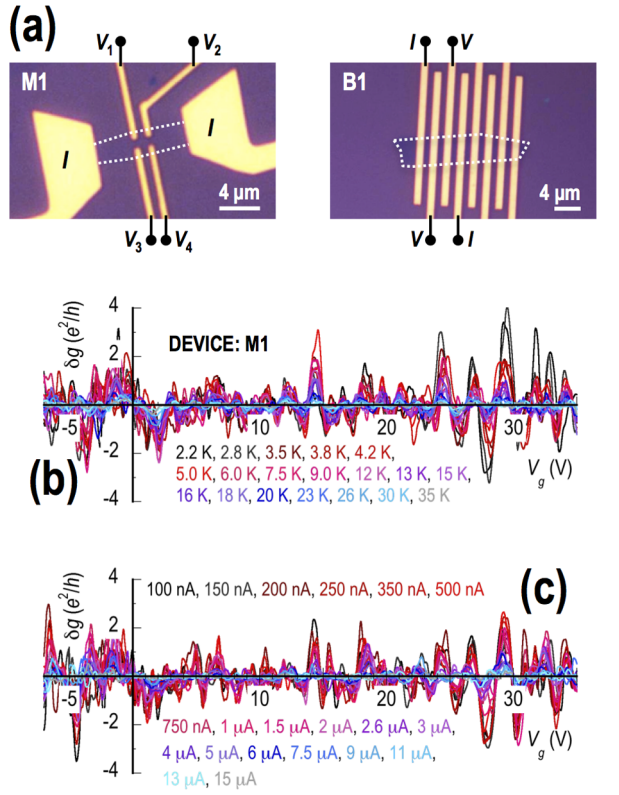

Figure 1. (a) Optical micrographs of two of the devices studied. White dotted lines indicate the position of the graphene flake and current and voltage probes are indicated. (b) Conductance fluctuations in device M1 as a function of gate voltage at various lattice temperatures (indicated). I = 100 nA RMS. (c) Corresponding fluctuations at a series of different RMS currents (indicated) for T_L = 1.8 K. In both (b,c), the fluctuations were obtained by subtracting a smooth background variation, as discussed in the Supporting Information.

Table 1. Important Parameters for the Different Devices Studied

device	L (μm)	W (μm)	L_p (μm)[a]	μ_h[b] (cm^2/(V s))	μ_e[b] (cm^2/(V s))	$k_F l$	D[c] (cm^2 s^{-1})
M1	10	2	0.8	7400	3800	5.3−19.8	500−532
B1	7	4	1	1050	1050	2.1−3.4	33−53
B2	6	0.25	4	1100	1200	2.0−3.1	32−50

[a] L_p: Voltage-probe separation. [b] μ_e, μ_h: Electron, hole mobility. [c] D: Diffusion coefficient.

input power required to achieve a given T_e, comparing the form of this with theoretical predictions. For an independent estimate of $T_e(I)$, we were also able to make use of the temperature dependence of the background conductance (which can be seen in the raw data shown in the Supporting Information), which provided values for T_e in close agreement with those determined from the CF. In the figures that follow, error bars in T_e predominantly reflect the difference between these two approaches.

In discussions of conventional semiconductors,[30−32] information on energy relaxation is typically obtained from the energy-loss rate (P_e), the average rate of energy loss per carrier[37] (we give a review of this in the Supporting Information). An important factor in this discussion is the T_{BG},[33,34] the value of T_L at which the energy of the largest-wavevector phonon is comparable to the carrier temperature.

dx.doi.org/10.1021/nl4020777 | Nano Lett. 2013, 13, 4305−4310

Since the largest-momentum phonon that can be emitted by the carriers is equal to $2k_F$, this temperature is defined as $T_{BG} = 2\hbar s k_F/k_B$, where s is the sound velocity and k_F is the Fermi radius. Taking $s = 2.1 \times 10^4$ ms^{-1} for graphene, $T_{BG} \sim 54n^{1/2}$ K (with n in units of 10^{12} cm^{-2}).[28] As will be seen below, this implies that our experiments are performed exclusively in the low-temperature ($T_L < T_{BG}$) limit, where P_e usually is related to the electron and lattice temperatures as

$$P_e = A(T_e^p - T_L^p) \quad (1)$$

with constants A and p dependent upon the specific scattering mechanisms that govern energy relaxation. In the inset to Figure 2a, we plot the variation of P_e for device B1 as a function of T_e and for various gate voltages. The dotted lines in the log–log plot indicate different power-law variations of T_e, namely p = 2 (predicted for cooling via out-diffusion[23]), 3, and 4 (for acoustic phonon processes[7−10]). Clearly, the data follow neither a T^2 nor T^4 variation, appearing close instead to a T^3 dependence. In the main panel, to emphasize the connection to eq 1, we therefore replot this data with $T_e^3 - T_L^3$ as the abscissa. The dotted line corresponds to a linear relationship between the axes, indicating that the data, which are obtained on both the electron and hole sides of the DP, are indeed well described by p = 3. In Figure 2b, we indicate that similar T^3 scaling is obtained for all three devices despite different mobility values and probe configurations. In Figure 2c, we replot the data for device B1 to show the variation of T_e as a function of the total power ($P = I^2R$). Note in this plot how fixed total power translates to larger T_e near the DP, which can be explained by the fact that $P_e \to \infty$ as $n \to 0$.

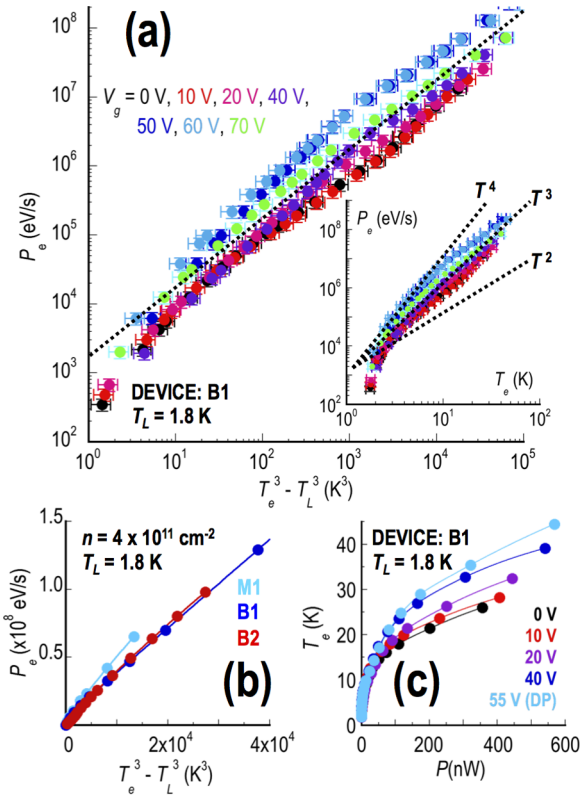

Figure 2. (a) The main panel plots the carrier power loss (P_e) as a function of ($T_e^3 - T_L^3$) for device B1 at different gate voltages (indicated) and at T_L = 1.8 K. The dotted line corresponds to a linear relation between the axes. Inset: same data as in the main panel, replotted with T_e as the abscissa. Dotted lines indicates various power-law relations. (b) Carrier power loss (P_e) as a function of ($T_e^3 - T_L^3$) for all three devices at an electron density of 4×10^{11} cm^{-2} and T_L = 1.8 K. (c) Variation of carrier temperature as a function of supplied power for device B1 at various gate voltages (indicated).

To determine the energy-relaxation time, we make use of the expression[1,32]

$$P_e = \frac{I^2R}{nWL} = \frac{k_B(T_e - T_L)}{\tau_\epsilon} \quad (2)$$

where W and L are the width and length of the graphene flake, respectively. In Figure 3a, we plot the variation of τ_ϵ as a function of density, for several measurement currents. (The shading denotes the region near the DP where the value of n cannot be verified directly from Hall measurements.) While results are shown for device B2, the variations in Figure 3a are quite generic to all three devices as can be seen from the comparison in Figure 3b. While it is tempting to conclude from this figure that the relaxation rate is typically faster in bilayer samples, caution is required here since these data were obtained for fixed current density and so do not correspond to equivalent T_e (see caption). In fact, we have thus far not been able to infer any conclusive dependence of the relaxation rate on layer structure. Further studies of larger ensembles of samples are likely required to resolve this issue, and for now the main feature that we emphasize is that energy relaxation in both

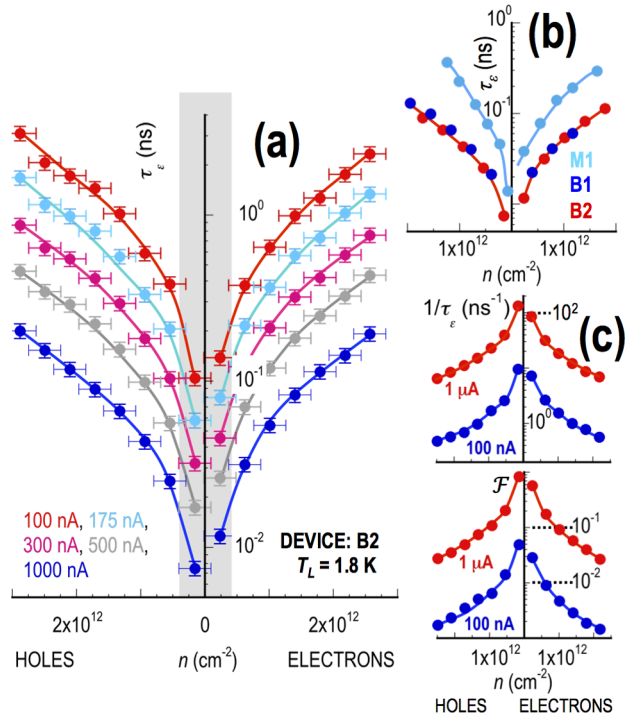

Figure 3. (a) Computed energy relaxation time for device B2 at T_L = 1.8 K, at various measurement currents (indicated). (b) Comparison of the density-dependent energy relaxation time for the three different devices. The data in this figure were obtained for a fixed current density of 2 μA/μm per graphene layer, for which $T_e \sim$ 11, 33, and 30 K for devices M1, B1, and B2, respectively. (c) Comparison of the energy-relaxation rate (top) and supercollision enhancement factor ($\mathcal{F}$, bottom)[13] for device B2. Solid lines through the data in (a–c) are a guide to the eye.

dx.doi.org/10.1021/nl4020777 | Nano Lett. 2013, 13, 4305−4310

monolayer and bilayer graphene becomes faster as the DP is approached.

Focusing on the behavior at any fixed n in Figure 3a, τ_ϵ shows a tendency to decrease with increasing current. That is, cooling occurs more quickly at higher currents, which can be understood by considering the temperature dependence of τ_ϵ shown in Figure 4. In Figure 4a, we plot $\tau_\epsilon(T_e)$ for device B2 on

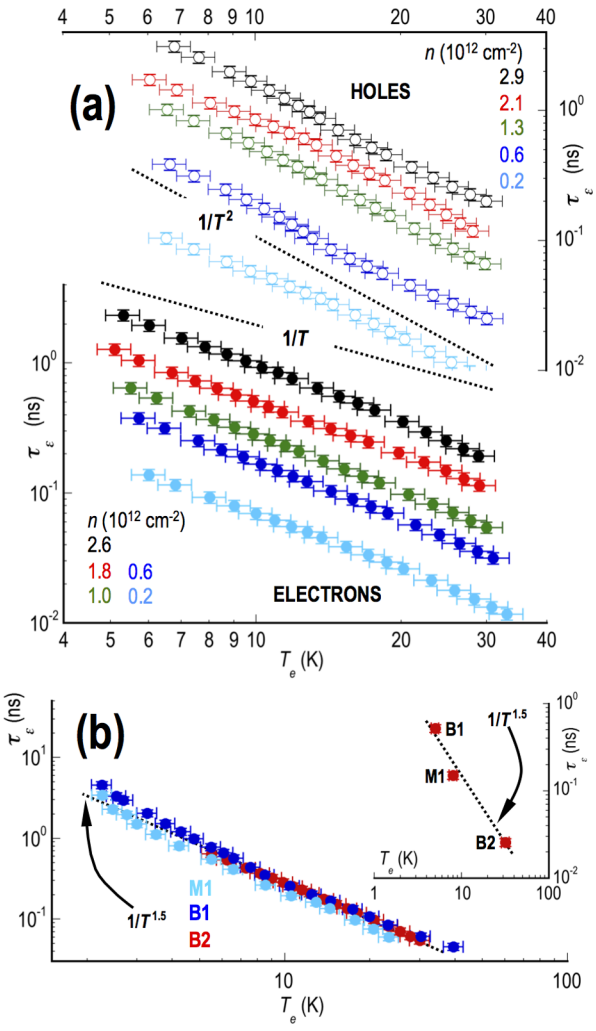

Figure 4. Temperature dependence of the energy-relaxation time. (a) Electron (bottom) and hole (top) energy-relaxation times. Data are for device B2, and corresponding electron/hole densities are indicated. Also indicated with dotted lines are different power-law variations. (b) Comparison of $\tau_\epsilon(T)$ for the three different devices. Gate voltage was adjusted to achieve an electron density of 1.2×10^{12} cm^{-2} in each device. The dotted line indicates a power-law variation of the form $T^{-3/2}$. Inset: Values of τ_ϵ and T_e are plotted at the Dirac point and for a current $I = 1$ μA RMS. A power-law variation of the form $T^{-3/2}$ is again indicated.

both the electron and hole sides of the DP. In all cases, τ_ϵ shows a power-law decay, close to $\tau_\epsilon \propto T^{-3/2}$, indicating that the decrease of this parameter with increasing current in Figure 3a can be attributed to heating of the carriers to higher T_e at larger currents. The generic character of this temperature decay is indicated in Figure 4b in which we compare the variation of $\tau_\epsilon(T)$ for all three devices. To provide a meaningful comparison here, the (electron) n was adjusted to 1.2×10^{12} cm^{-2} in each device, and the variations of $\tau_\epsilon(T)$ agree excellently with each other. An alternative way of representing this is presented in the inset to Figure 4b, which was obtained from DP data by determining for each device the value of τ_ϵ and T_e at a measurement current of 1 μA. Plotting these data on a common graph, we once again obtain a variation close to $\tau_\epsilon \propto T^{-3/2}$.

By far the most striking feature of our data in all three devices and at all measurement currents is the decrease of the relaxation time by more than an order of magnitude that occurs as the DP is approached from either side (Figures 3a,b). Such behavior is actually reminiscent of recent theories for energy relaxation due to acoustic-phonon scattering, which yield a relaxation time that varies close to $\tau_\epsilon \propto n^{1/2}$ in both clean[8] and disordered[13] graphene. In ref 8, this conclusion was reached after applying a low-temperature approximation to the Fermi distribution and calculating carrier cooling via unscreened acoustic deformation-potential coupling. In the limit of vanishing transferred phonon momentum, the energy-loss rate was found to vary as $\sim E_F/n \propto n^{-1/2}$ (where E_F is the Fermi energy), diverging as the DP is approached. This surprising result was explained by noting that the relaxation rate $\tau_\epsilon^{-1} \sim (1/C_e)(dP/dT_e)$, where C_e is the electronic specific heat and is therefore proportional to the density of states. Since the latter vanishes as the DP is approached in graphene, the relaxation rate should therefore simultaneously diverge (i.e., $\tau_\epsilon \rightarrow 0$). A similar conclusion was reached, albeit within a very different model in ref 13 where impurity-mediated "supercollisions" were also predicted to yield an energy-loss rate $P_e \propto T^3$, reminiscent of the behavior in Figure 2. Despite this, there are a number of other factors that suggest that the variations of τ_ϵ that we observe are inconsistent with the theories of either refs 8 or 13. First, the quantitative scaling of $\tau_\epsilon(n)$ that we find near the DP is stronger than the $n^{1/2}$ dependence predicted in refs 8 and 13 (see Supporting Information for more details). Second, while supercollisions are predicted[13] to dominate at high temperatures ($T_L > T_{BG}$), our experiments are actually performed in the opposite regime ($T_L < T_{BG}$) where they should not be dominant. To emphasize this point, we determine the enhancement factor ($\mathcal{F}$)[13] that gives the strength of the supercollisions relative to direct, phonon-mediated, scattering

$$\mathcal{F} = \frac{0.77}{k_F l}\frac{(T_e^2 + T_e T_L + T_L^2)}{T_{BG}^2} \qquad (3)$$

where l is the mean-free path. In Figure 3c, we plot the energy-relaxation rate (τ_ϵ^{-1}) along with the variation of $\mathcal{F}$ determined for our data. Results are plotted for two measurement currents and, while the qualitative variations of τ_ϵ^{-1} follow those of $\mathcal{F}$ closely, the value of $\mathcal{F}$ is always less than one. In other words, for the range of densities that we consider supercollisions would only be expected to lead to no more than a doubling of the relaxation rate, a change that is too small to account for the order-of-magnitude variations of τ_ϵ in Figure 3. Consistent with this, we also note that the power-law decay of τ_ϵ ($\propto T^{-3/2}$) in Figure 4 is distinct to that ($\propto T^{-1}$) reported[27] for supercollisions.

Having suggested that our results are inconsistent with existing theories for phonon-mediated energy relaxation, we note that the presence of the CF we use as a thermometer points to the disordered nature of the graphene. In the presence of this, the system is known to break up into puddles of localized electrons and holes,[38−41] a unique state that is characterized by strong incompressibility at and around the

dx.doi.org/10.1021/nl4020777 | Nano Lett. 2013, 13, 4305−4310

DP.[42−44] The incompressibility indicates that the puddle state becomes almost "frozen" into the system, much as the vapor pressure is reduced over a frozen liquid. Since the power-per-carrier increases as the DP is approached, the suggestion is that the associated decrease of τ_ϵ is somehow a self-consistent consequence of the incompressibility. The essential point is that the decrease of τ_ϵ avoids a divergence of T_e (see eq 2), which would correspond to strong delocalization of carriers out of their puddles, violating the notion of their incompressibility.

In conclusion, we have studied current-induced heating of carriers in graphene, determining the energy-relaxation time on both the electron and hole sides of the Dirac point. While the power law behavior of the power input appears suggestive of a connection to supercollision scattering, the size of the effect and the dependence of the relaxation time on temperature and density do not support this process. The dramatic collapse of the relaxation time near the Dirac point may be consistent with ideas of charge puddling, by suggesting that it becomes very difficult to excite carriers out of these localized regions. While we are unable to comment at this stage on the influence of the graphene layer structure on quantitative relaxation rates, we have found that both monolayer and bilayer devices show the same trend for faster cooling as the DP is approached. This at least suggests that this variation of the relaxation time does not require the presence of linear bands, but that it is rather more closely related to the vanishing of the density of states as the DP is approached. In fact, the similar trends obtained for monolayer and bilayer graphene are consistent with our assertions concerning the dominance of puddle formation in the presence of disorder. In this sense, it would be of interest in the future to investigate energy relaxation in clean graphene, in which the role of the different bandstructures might be more apparent.

■ ASSOCIATED CONTENT

Supporting Information

Description of basic devices characterization and hot-carrier thermometry. This material is available free of charge via the Internet at http://pubs.acs.org.

■ AUTHOR INFORMATION

Corresponding Author

*E-mail: jbird@buffalo.edu; Phone: +1 (716) 645-1015.

Author Contributions

The authors contributed equally to this work.

Notes

The authors declare no competing financial interest.

■ ACKNOWLEDGMENTS

This research was supported by the U.S. Department of Energy, Office of Basic Energy Sciences, Division of Materials Sciences and Engineering under Award DE-FG02-04ER46180 (G.B. and J.P.B.), and the National Science Foundation under Award OISE0968405 (R.S.).

■ REFERENCES

(1) Ferry, D. K. *Semiconductor Transport*; Taylor & Francis: London, 2000.

(2) Sze, S. M; Lee, M. K. *Semiconductor Devices: Physics and Technology*, 3rd ed.; John Wiley and Sons: Hoboken, NJ, 2012.

(3) Meric, I.; Han, M. Y.; Young, A. F.; Ozyilmaz, B.; Kim, P.; Shepard, K. L. *Nat. Nanotechnol.* **2008**, *3*, 654−659.

(4) Freitag, M.; Steiner, M.; Martin, Y.; Perebeinos, V.; Chen, C.; Tsang, J. C.; Avouris, P. *Nano Lett.* **2009**, *9*, 1883−1888.

(5) Barreiro, A.; Lazzeri, M.; Moser, J.; Mauri, F.; Bachtold, A. *Phys. Rev. Lett.* **2009**, *103*, 076601.

(6) DaSilva, A. M.; Zou, K.; Jain, J. K.; Zhu, J. *Phys. Rev. Lett.* **2010**, *104*, 236601.

(7) Bistritzer, R.; MacDonald, A. H. *Phys. Rev. Lett.* **2009**, *102*, 206410.

(8) Kubakaddi, S. *Phys. Rev. B* **2009**, *79*, 075417.

(9) Tse, W. K.; Das Sarma, S. *Phys. Rev. B* **2009**, *79*, 235406.

(10) Viljas, J. K.; Heikkilä. *Phys. Rev. B* **2010**, *81*, 245404.

(11) Song, J. C. W.; Rudner, M. S.; Marcus, C. M.; Levitov, L. S. *Nano Lett.* **2011**, *11*, 4688−4692.

(12) Low, T.; Perebeinos, V.; Kim, R.; Freitag, M.; Avouris, P. *Phys. Rev. B* **2012**, *86*, 045413.

(13) Song, J. C. W.; Reizer, M. Y.; Levitov, L. S. *Phys. Rev. Lett.* **2012**, *109*, 106602.

(14) Chen, W.; Clerk, A. A. *Phys. Rev. B* **2012**, *86*, 125443.

(15) Plochocka, P.; Kossacki, P.; Golnik, A.; Kazimierczuk, T.; Berger, C.; de Heer, W. A.; Potemski, M. *Phys. Rev. B* **2009**, *80*, 245415.

(16) Voutilainen, J.; Fay, A.; Häkkinen, P.; Viljas, J. K.; Heikkilä, T. T.; Hakonen, P. J. *Phys. Rev. B* **2011**, *84*, 045419.

(17) Tan, Z.; Tan, C.; Ma, L.; Liu, G. T.; Lu, L.; Yang, C. L. *Phys. Rev. B* **2011**, *84*, 115429.

(18) Gabor, N. M.; Song, J. C. W.; Ma, Q.; Nair, N. L.; Taychatanapat, T.; Watanabe, K.; Taniguchi, T.; Levitov, L. S.; Jarillo-Herrero, P. *Science* **2011**, *334*, 648−652.

(19) Sun, D.; Aivazian, G.; Jones, A. M.; Ross, J. S.; Yeo, W.; Cobden, D.; Xu, X. *Nat. Nanotechnol.* **2012**, *7*, 114−118.

(20) Baker, A. M. R.; Alexander-Webber, J. A.; Altebaeumer, Y.; Nicholas, R. J. *Phys. Rev. B* **2012**, *85*, 115403.

(21) Price, A. S.; Hornett, S. M.; Shytov, A. V.; Hendry, E.; Horsell, D. W. *Phys. Rev. B* **2012**, *85*, 161411(R).

(22) Yan, J.; Kim, M. H.; Elle, J. A.; Sushkov, A. B.; Jenkins, G. S.; Milchberg, H. M.; Fuhrer, M. S.; Drew, H. D. *Nat. Nanotechnol.* **2012**, *7*, 472−478.

(23) Betz, A. C.; Vialla, F.; Brunel, D.; Voisin, C.; Picher, M.; Cavanna, A.; Madouri, A.; Fève, G.; Berroir, J.-M.; Plaçais, B.; Pallecchi, E. *Phys. Rev. Lett.* **2012**, *109*, 056805.

(24) Fong, K. C.; Schwab, K. C. *Phys. Rev. X* **2012**, *2*, 031006.

(25) Majumdar, K.; Kallatt, S.; Bhat, N. *Appl. Phys. Lett.* **2012**, *101*, 123505.

(26) Baker, A. M. R.; Alexander-Webber, J. A.; Altebaeumer, T.; McMullan, S. D.; Janssen, T. J. B. M.; Tzalenchuk, A.; Lara-Avila, S.; Kubatkin, S.; Yakimova, R.; Lin, C.-T.; Li, L.-J.; Nicholas, R. J. *Phys. Rev. B* **2013**, *87*, 045414.

(27) Graham, M. W.; Shi, S.-F.; Ralph, D. C.; Park, J.; McEuen, P. L. *Nat. Phys.* **2013**, *9*, 103−108.

(28) Betz, A. C.; Jhang, S. H.; Pallecchi, E.; Ferreira, R.; Fève, G.; Berroir, J.-M.; Plaçais, B. *Nat. Phys.* **2013**, *9*, 109−112.

(29) Sun, D.; Divin, C.; Berger, C.; de Heer, W. A.; First, P. N.; Norris, T. B. *Phys. Status Solidi C* **2011**, *8*, 1194−1197.

(30) Stöger, G.; Brunthaler, G.; Bauer, G.; Ismail, K.; Meyerson, B. S.; Lutz, J.; Kuchar, F. *Phys. Rev. B* **1994**, *49*, 10417.

(31) Fletcher, R.; Feng, Y.; Foxon, C. T.; Harris, J. J. *Phys. Rev. B* **2000**, *61*, 2028−2033.

(32) Prasad, C.; Ferry, D. K.; Vasileska, D.; Wieder, H. H. *Physica E* **2003**, *19*, 215−220.

(33) Efetov, D. K.; Kim, P. *Phys. Rev. Lett.* **2010**, *105*, 256805.

(34) Fuhrer, M. S. *Physics* **2010**, *3*, 106.

(35) Bohra, G.; Somphonsane, R.; Aoki, N.; Ochiai, Y.; Akis, R.; Ferry, D. K.; Bird, J. P. *Phys. Rev. B* **2012**, *86*, 161405(R).

(36) Bohra, G.; Somphonsane, R.; Aoki, N.; Ochiai, Y.; Ferry, D. K.; Bird, J. P. *Appl. Phys. Lett.* **2012**, *101*, 093110.

(37) Yu, P. Y.; Cardona, M. *Fundamentals of Semiconductors: Physics and Materials Properties*, 3rd ed.; Springer-Verlag: Berlin, 2005.

(38) Hwang, E. H.; Adam, S.; Das Sarma, S. *Phys. Rev. Lett.* **2007**, *98*, 186806.

(39) Adam, S.; Hwang, E. H.; Galitski, V. M.; Das Sarma, S. *Proc. Natl. Acad. Sci. U.S.A.* **2007**, *104*, 18392−18397.
(40) Tan, Y.-W.; Zhang, Y.; Bolotin, K.; Zhao, Y.; Adam, S.; Hwang, E. H.; Das Sarma, S.; Stormer, H. L.; Kim, P. *Phys. Rev. Lett.* **2007**, *99*, 246803.
(41) Chen, J.-H.; Jang, C.; Adam, S.; Fuhrer, M. S.; Williams, E. D.; Ishigami, M. *Nat. Phys.* **2008**, *4*, 377−381.
(42) Martin, J.; Akerman, N.; Ulbricht, G.; Lohmann, T.; Smet, J. H.; Von Klitzing, K.; Yacoby, A. *Nat. Phys.* **2008**, *4*, 144−148.
(43) Martin, J.; Feldman, B. E.; Weitz, R. T.; Allen, M. T.; Yacoby, A. *Phys. Rev. Lett.* **2010**, *105*, 256806.
(44) Young, A. F.; Dean, C. R.; Meric, I.; Sorgenfrei, S.; Ren, H.; Watanabe, K.; Taniguchi, T.; Hone, J.; Shepard, K. L.; Kim, P. *Phys. Rev. B* **2012**, *85*, 235458.